Physics of the Earth and Planetary Interiors 344 (2023) 107090

Contents lists available at ScienceDirect

Physics of the Earth and Planetary Interiors

journal homepage: www.elsevier.com/locate/pepi

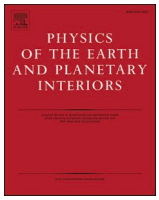

A grand spectrum of the geomagnetic field

Catherine Constable *, Steven Constable

Cecil H. and Ida M. Green Institute of Geophysics & Planetary Physics, Scripps Institution of Oceanography, University of California San Diego, 9500 Gilman Drive, La Jolla, CA 92093-0225, USA

ARTICLE INFO

Keywords:
Geomagnetic field
Power spectrum
Magnetic field variations through time

ABSTRACT

The spectrum of geomagnetic variations is broad and reflects multiple internal and external physical Earth processes. The geodynamo generates an internal magnetic field, dominated by the low frequency contribution of the axial dipole whose temporal variations range from geomagnetic reversals, excursions, and large-scale paleosecular variations, down to decadal and sub-annual changes. Variations in the external field arise from high frequency interactions of the solar wind with Earth's magnetosphere and ionosphere, along with excitation within the atmospheric cavity by lightning, power systems, and radio transmissions. External variations induce a field in the conductive Earth that adds to the internal signal. A spherical harmonic analysis of dipole terms in over 100 years of observatory data allows us to show that the external field is stronger than the internal field at periods of the 11-year sunspot cycle and shorter. Using spectral estimates derived from this and other data sets by adaptive multi-spectral time series analysis, we can create a composite power spectrum that spans frequencies from 10^{-15} Hz to 20 kHz (periods ranging from 10 million years to 5×10^{-5} s), and powers ranging from 10^{-9} $(\mathrm{nT})^2/\mathrm{Hz}$ to 10^{21} $(\mathrm{nT})^2/\mathrm{Hz}$. The different processes contributing to the spectrum are characterized by various inverse power laws across frequency bands. This Grand Spectrum quantifies the successive dominance of the many different geophysical processes with frequency, but importantly provides a compelling graphic to illustrate the complexity of the geomagnetic field.

1. Introduction

Earth's magnetic field varies over a vast span of time scales, from reversals of the internally-generated main core field (at an average but highly irregular rate of around 2 per million years for the past 160 My), to natural and anthropogenic external radio signals at kilohertz frequencies. Table 1 lists the various contributions to the field as it is measured at Earth's surface. Both the internal and external fields follow a generally red spectrum, with piecemeal approximate background power laws that range from f^{-6} to f^0 across the 20 orders of magnitude span in frequency, and produce about 30 orders of magnitude decrease in power.

Early efforts to obtain power spectra from magnetic observatory data started in the early 1960's, when digital computers began to be used for Fourier analysis. The first paper on this subject appears to be that of Eckhardt et al. (1963), who estimated spectral peaks for six harmonics of the daily variation, the first harmonic of the 27-day solar rotation period, and 6 months. Banks and Bullard (1966) added the one year and the 27-day fundamental, and Banks (1969) presented a hand-drawn spectrum showing all these peaks but with an obviously incorrect flat background spectrum. The paper by Lanzerotti et al. (1990) is notable for presenting two spectra from Antarctica that span 10^{-5} to 10^5 Hz. More recently Olsen (2007) shows a composite spectrum derived from observatory data from 10^{-8} to 10^3 Hz. Paleomagnetic spectral estimation had its infancy during the 1980s, when Barton (1982) began by looking at directional records from lake sediments and Courtillot and Le Mouël (1988) made early attempts to synthesize power laws for spectra extending from about 1 h to around 1 million year periods.

Constable and Constable (2004) extended these preliminary efforts to much longer periods and introduced the "Grand Spectrum", attempting to capture all the important variations of the dipole field and their underlying physics in a single image of the magnetic field spectrum. Their figure relied on re-drawing spectra from others' work, contained gaps, and lacked uncertainty measures. The spectrum in the frequency overlap between the internally generated core field and the externally generated magnetospheric field was not well documented, nor was the externally induced internal field considered. However, the graphic became a useful pedagogical tool and reference model

* Corresponding author.
E-mail address: cconstable@ucsd.edu (C. Constable).

https://doi.org/10.1016/j.pepi.2023.107090
Received 3 May 2023; Received in revised form 30 July 2023; Accepted 23 August 2023
Available online 28 August 2023

Table 1
Typical properties of various geomagnetic variations.

Type of Variation	Symbol	Period or Frequency	Amplitude
Reversals/Excursions		2–10/My	50 000 nT
Paleosecular Variation		100 y-100 ky	100–30 000 nT
Secular Variation		1-100 y	10–1000 nT
Solar Cycle		11 years	
Annual		12 months	
Semiannual		6 months	
Solar rotation		27 d and harmonics	
Storm-time	Dst	hours to weeks	50–500 nT
Regular Daily			
at mid-latitudes	Sq	24 h and harmonics	20–50 nT
at low latitudes	EEJ	12 h	50–100 nT
Substorms	DP	10 min to 2 h	100 nT (1000 nT at p. l.)
Pulsations	ULF	0.3-600 s	
regular	pc	150-600 s (pc5)	10 nT(100 nT at p.l.)
continuous		45-150 s (pc4)	2 nT
pulsations		5-45 s (pc2,3)	0.5 nT
		0.2-5 s (pc1)	0.1nT
Schumann Resonances		8 Hz and harmonics	<0.1 nT
Extreme low frequency	ELF Sferics	3 Hz- 3 kHz	<0.1 nT
Powerline, anthropogenic		50 Hz +	variable

p.l. is for polar latitude dependence with values for latitudes $> 65°$).

(Constable, 2016; Constable, 2019), capturing a huge amount of complexity in a single figure.

Here we produce an updated version of the Grand Spectrum, using a reproducible work flow and making the underlying time series and derived spectra available in digital form. We highlight the spectral transition, between periods of 11 years and one day, where Earth's magnetic field undergoes changes from dominance by the internally generated core field to the external magnetospheric, ionospheric, and atmospheric field. One important part of the magnetic field, the lithospheric field produced by induced and remanent magnetization of magnetic minerals, is not considered in this study because any time variations in magnetization associated with tectonic activity and weathering are at such long periods that the main core field dominates.

2. Methods

How does one measure the amplitude of the magnetic field when some measurements are derived from paleomagnetic data bases, some from the global magnetic observatory network, and some from individual induction coil sensors? This question is further complicated by the fact that magnetic fields vary spatially as well as temporally. In the simplest approximation as a dipole form, the amplitude of Earth's field is twice as large at the poles as it is at the equator. However, the field that Earth's core generates is more complex than a simple dipole, and these complexities are themselves subject to temporal variation. The use of spectral analysis supposes that time variations in the field can be considered stationary, which loosely speaking implies that the statistical representation of the physics doesn't change over time. This is not generally true of Earth's magnetic field, with one dramatic example being magnetic storms caused by sudden changes in the number of solar particles reaching Earth's magnetosphere. Nevertheless, the power spectrum provides a useful description that helps separate the broad range of processes that contribute to the measured field. The paleomagnetic and observatory data are fit with mathematical models that use spherical harmonics to describe the spatial geometry of the field, and allow the harmonic coefficients to vary with time to capture secular variation. The paleofield models include structure in coefficients up to about degree and order 4, while the recent observatory models, which include data from magnetic satellites, extend to degree and order 13. These models are important for understanding core dynamics and have practical use in navigation, but fortunately, in constructing a power spectrum that varies over 30–40 orders of magnitude, most details can be left to the specialists who study specific parts of the system and how they work. We consider only the largest spatial scales as recorded in paleomagnetic field reconstructions and geomagnetic field models of the scalar magnetic potential based on direct observations. Also, it is worth noting that in paleofield models the secular variation in the dipole term, which is what the spectrum captures, is relatively large compared with the secular variation in the higher order harmonics.

We extract time series of the axial dipole moment as specified by spherical harmonic coefficients of degree one and order zero. In geomagnetic and paleomagnetic field models this is commonly termed g_1^0 for the internal part of the field and follows a $P_1^0(\cos\theta)$ spatial structure for the potential field (e.g., Backus et al., 1996), with P_1^0 a Schmidt-normalized associated Legendre function, and θ the colatitude in a geocentric coordinate system. The magnetic field is given by the gradient of the potential. On time scales up to about a century we can use magnetic observatory records and recover separately the external and internal field contributions to the gradient of a P_1^0 spherical harmonic function. The observatory index, SYM-H, assesses mid-latitude total horizontal fields with 1-min sampling. For the highest frequencies, we use magnetic induction coil measurements collected during magnetically quiet times from a single mid-latitude site which is also relatively quiet with respect to anthropogenic noise, and include an example of data collected during a magnetic storm for comparison.

We derive power spectral estimates using the adaptive sine multitaper algorithm of Riedel and Sidorenko (1995, 1996), which adjusts the amount of spectral averaging based on the details of structure present in the spectrum at a given frequency. Because the number of tapers varies with frequency, the error in the spectrum is also dependent on frequency, and will reflect the usual tradeoff between resolution and bias. Further details can be found in Constable and Johnson (2005).

Spectra are functions of frequency, although period can also be used, and broad spectrum processes are invariably plotted on a logarithmic scale. Per million years is a useful frequency to use for paleomagnetic records, but not so useful for power-line frequencies. Since there is no practical unit that will span the Grand Spectrum, we will use the SI unit of frequency, Hz, and annotate the plots with more relatable units such as years and days.

The original Grand Spectrum (Constable and Constable, 2004) was presented as an amplitude spectrum, but a power spectral density estimate is a measure of variance, or power, normalized by bandwidth in frequency. The SI unit would thus be T^2/Hz, but a Tesla is a large field and the biggest geophysically relevant fields at Earth's surface are too small to even exceed one mT. Observatory records are reported in nT, a unit that we hope most readers will find relatable: our time series are made available in nT and our spectra are reported in nT^2/Hz.

The Grand Spectrum is necessarily constructed piecemeal, 4–5 decades at a time from a range of data sources, and Fig. 1 shows the complete product with annotations about the contributing processes (see also Table 1). In the rest of this paper we discuss the piecewise derivation and assembly of the Grand Spectrum, starting from the longest periods representing geomagnetic reversals and long term paleosecular variation and progressing to the highest frequencies where anthropogenic effects are clearly visible.

3. Geomagnetic and paleomagnetic field models and proxies

Substantial progress in geomagnetic and paleomagnetic field modeling has occurred over the past three decades as available data have greatly increased in number, quality, and spatial distribution. The

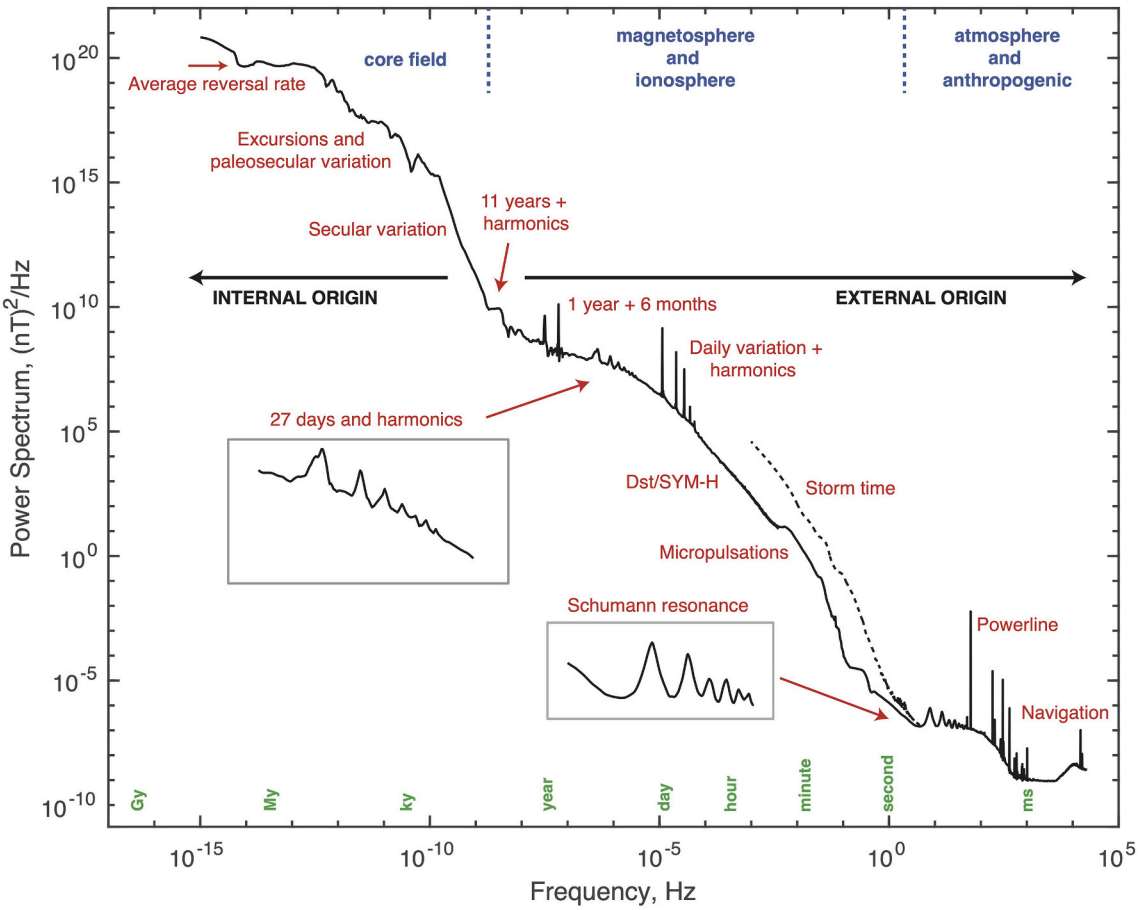

Fig. 1. The Grand Spectrum of the geomagnetic field, based on global observations of the geomagnetic dipole at periods greater than one minute and local observations of the horizontal field at shorter periods. .

implementation of regularized inversion techniques (e.g., Constable et al., 1987) enforcing minimal complexity in spatial and temporal variations has enabled the construction of numerous time-varying spherical harmonic models of varying resolution and length (e.g., Jackson et al., 2000; Gillet et al., 2013; Panovska et al., 2019; Alken et al., 2021). Direct geomagnetic observations in the form of data from satellites and geomagnetic observatories are used to produce models that span the satellite era (here we focus on *CHAOS7.9* for 1999–2020 CE of Finlay et al. (2020)) and the historical global observatory model *COV-OBS.x2* (covering 1840–2020 CE, Huder et al. (2020)) that uses land survey and maritime data, annual means from observatories as in Jackson et al. (2000) and other direct measurements of the field available from 1840 CE on. Moving beyond the direct record we select a suite of 3 time-varying spherical harmonic models made from paleomagnetic data: *ARHIMAG1k* (Senftleben, 2020) is derived from both archeomagnetic and historical observations from 800–1990 CE; *HFM.OL1.A1* (Constable et al., 2016) covers the interval 0–10 ka with paleomagnetic data; *GGF100k* extends from 0–100 ka (Panovska et al., 2018). A review of paleofield modeling extending to 100 ka is given by Panovska et al. (2019). From each of these models we extracted time series of the absolute value of the leading spherical harmonic coefficient $|g_1^0|$ in nT as representative of variations in the axial-dipole moment.

Before 100 ka there is not yet a longer time-varying spherical harmonic representation for the geomagnetic field. We make use of *PADM2M*, a measure of axial dipole moment variations over 0–2 Ma based on globally distributed sedimentary relative paleointensity variations calibrated using absolute paleointensity data from the same period (Ziegler et al., 2011). In both PADM2M and the spherical harmonic models the time variations are parameterized in terms of order 4 B-splines, except for CHAOS7 which uses order 6 splines. The spline knot spacings range from 0.5 years for CHAOS7 to 1000 years for PADM2M (see Table 2 for further details).

At still longer timescales, extending to 158 Ma, we do not have detailed knowledge of temporal variations in field strength, but there is a reliable record of geomagnetic polarity and transition ages drawn from seafloor magnetic anomalies, which we call *GTS12* after the geomagnetic time scale of Ogg et al. (2012). Following the strategy of Constable

Table 2
Time span, sampling interval or rate, minimum and maximum frequency resolution, and frequency range used for the Grand Spectrum compilation, in practical units. Note that the COV-OBS and CHAOS7 internal fields, shown in Fig. 2, are not part of the Grand Spectrum because external dipole fields dominate at those frequencies.

Description	Time Span/ Length	Samp. ΔT	Δf_{min}-Δf_{max}	Frequency Range
GTS12	0–157.8 Ma	n/a	0.18–3.3/My	0.03–16/My
PADM2M	0–2 Ma	1000 y	6.5–16/My	0.016–0.11/ky
GGF100k	0–100 ka	100 y	0.09–0.09/ky	0.11–0.62/ky
HFM.OL1.A1	0–10 ka	20 y	0.62–1.1/ky	0.62–4/ky
ARHIMAG1k	1000–2000 CE	5 y	17–28/ky	5–56/ky
COV-OBS Int.	1840–2020 CE	1 y	17–33/ky	–
CHAOS7 Int.	1999–2020 CE	1 y	0.125–0.25/y	–
Observatory	1903–2021 CE	1 h	0.07–18.5/y	0.05–1843/y
SYM-H	2015–2022 CE	60 s.	0.01–0.05/hour	0.21–13.68/hour
Borrego	2 days	5 Hz	0.002–0.024 Hz	0.004–0.165 Hz
Borrego	2 h	500 Hz	0.07–1.67 Hz	0.165–202 Hz
Quasar	50 s	40 kHz	14–87 Hz	0.202–20 kHz
Storm	12 h	50 Hz	0.007–0.26 Hz	0.001–4 Hz

et al. (1998) we use GTS12 as a proxy, invoking a simple model that supposes the axial dipole strength is constant at the average value of PADM2M during stable polarity time and drops to zero throughout a reversal to produce a time series extending back to 158 Ma.

In an earlier paper, Sadhasivan and Constable (2022) used several of these records (GTS12, PADM2M, GGF100k, HFM.OL1.A1, ARHIMAG1k) together with *CALS10k.2* (Constable et al., 2016) and the interval of *gufm1* covered by intensity records (Jackson et al., 2000) to produce an empirical paleomagnetic power spectrum for the axial-dipole moment. Here we discard CALS10k.2 which essentially duplicates the HFM.OL1.A1 record, replace the truncated version of *gufm1* with the more recent and slightly longer COV-OBS.x2, and augment the high frequency internal core field spectrum with CHAOS7.9. The updated spectrum for the core field, $|g_1^0|$, is shown in Fig. 2. Sadhasivan and Constable (2022) found that the trend in their observed power spectrum exhiPEPId three distinct regimes transitioning from an essentially flat spectrum consistent with random reversal occurrences to power law of spectral falloffs as f^{-n} with $n = 2, 4, 6$ at corner frequencies corresponding to 10.91/My, 5.44/ky and 83/ky as indicated on Fig. 2.

4. Hourly magnetic observatory data

Hourly magnetic observatory data have been collected for more than 100 years, and so provide a relatively long time series that can bridge the gap between satellite and historical/archaeomagnetic records that focus on the core field, and the high frequency campaign style measurements described in subsequent sections of this paper. However, the number and location of observatories varies in time as they are commissioned, decommissioned, or moved. Although a handful of observatories have effectively been operating since the early 1900's, applying baseline changes after small geographic moves and instrument changes, inevitably there are periods when no data are reported, so no observatory has been recording without interruption for 100 years. As is the case for the paleo- and historical data, external variations at periods between one day and about 11 years are largely dipolar in geometry and so will have a latitudinal dependence. This is because the external field at these periods is mostly generated by magnetospheric currents trapped in the radiation belts, fed by particles injected from the solar wind, particularly during magnetic storms (Daglis et al., 2007). These currents flow in a torus around Earth between 2 and 9 Earth radii, generating a largely

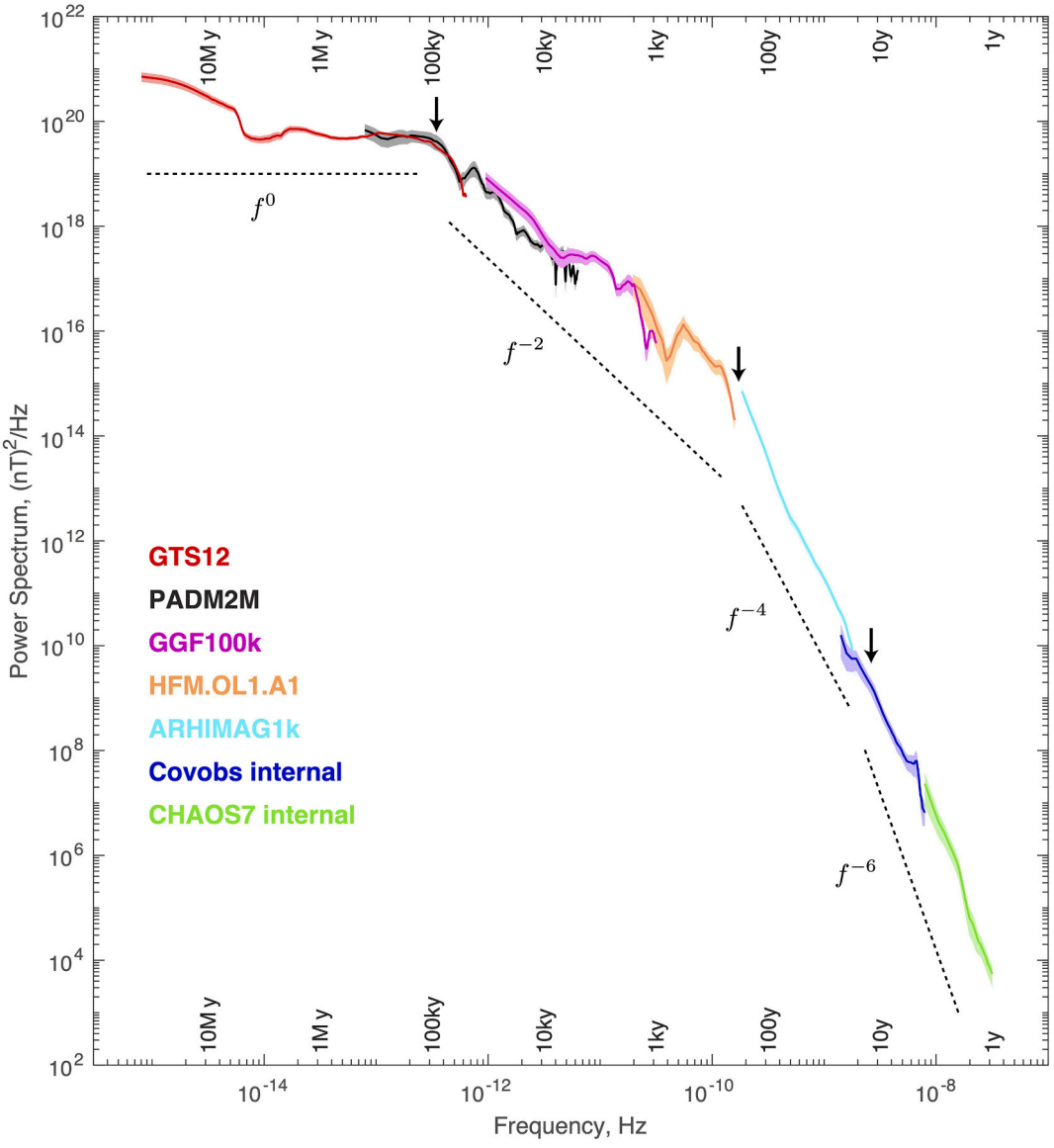

Fig. 2. Composite power spectrum of internal geomagnetic axial-dipole variations, $|g_1^0|$ based on time series of Table 2. Lighter colors deNote 1 standard error range. Vertical black arrows mark transition frequencies in power law dependence from Sadhasivan and Constable (2022).

dipolar field. Because magnetic storms are modulated by the 11-year solar cycle, we can expect this geometry to be dominant out to that period. The exception is the narrow annual and 6-month peaks in the spectrum, which have a more complicated geometry. By continuing to characterize the field by its dipole moment, or P_1^0 spherical harmonic coefficient, we can expect to provide a spectral estimate that is consistent with the global paleofield models.

The period band covering 1–11 years is also the region where secular variation of the internal core field becomes overwhelmed by external field variations driven by the solar wind, radiation belts, and daily solar heating of the ionosphere. Large scale internal fields generated by the core geodynamo are attenuated at Earth's surface by the filtering effect of lower mantle conductivity, with a delay time estimated to be between about 0.5 and 4 years (Backus, 1983; Pinheiro and Jackson, 2008). Although variations in the core field as short as several months are identified as occasional "geomagnetic jerks" (Mandea et al., 2010), or abrupt changes in the second time derivative of the field components in some observatories, these phenomena are too small to be evident in the long-term spectrum of the dipole field. It is important to note at this point that the COV-OBS and CHAOS models exclude data during magnetic storms, because they constitute noise when trying to characterize the internal core field (the subject of the previous section of this paper). However, as we move to the shorter period parts of the spectrum, magnetic storms become an important, even dominant, component of the spectrum, and therefore must be included in our analysis.

External field variations can reasonably be expected to extend from short periods to at least the 11-year sun-spot cycle, and will induce an internal field which depends on Earth's electrical conductivity and period. It is therefore useful to separate the spectra into internal and external components in the observatory frequency band. In a geocentric coordinate system the radial (outward vertical) magnetic field data is designated B_r and horizontal (southward) magnetic field data B_θ. Here we use this notation to represent the vector residual after the main core field has been removed. Each is a function of colatitude θ for a given time (a given hour in this case), and for globally distributed values the induced internal, $i_1^0(t)$, and external $e_1^0(t)$ axial dipole coefficients are given by least squares solution of the following equations

$$\begin{bmatrix} -\cos(\theta) & 2(a/r)^3\cos(\theta) \\ \sin(\theta) & (a/r)^3\sin(\theta) \end{bmatrix} \begin{bmatrix} e_1^0 \\ i_1^0 \end{bmatrix} = \begin{bmatrix} B_r \\ B_\theta \end{bmatrix} \quad (1)$$

where geocentric radius, r, is determined by observatory altitude above a, the average Earth radius (6371.2 km). Since the best fitting dipole is tilted from Earth's rotation axis, the fit is better if the system is rotated into geomagnetic dipole coordinates based on the IGRF, which we do year by year to track the migration of the geomagnetic poles.

There are several assumptions made in using this approach. The one-year, six month, and diurnal variations in the external magnetic field are known to be more complicated than a simple dipole – we discuss this below. The dipole geometry of the external field during geomagnetic storms is derived from the "ring current" in the radiation belts, which is known to have some asymmetry between night and day sides of Earth (Balasis and Egbert, 2006), but this is a second order effect and Balasis and Egbert (2006) note that only the axisymmetric part of the external field will contribute to long-period induction. For the induced field to also be dipolar, Earth's electrical conductivity structure must be radially symmetric, which is a good approximation given that temperature and pressure are the main drivers of conductivity. The largest departure from radial conductivity comes from the oceans, which can affect the vertical magnetic field at periods shorter than about 2 days for coastal observatories (Everett et al., 2003; Olsen and Kuvshinov, 2004). In the early parts of the observatory record there are only a few observatories reporting, mostly from Europe, which would make separating P_1^0 for higher order harmonics difficult, but if the field is assumed *a priori* to be dipolar the use of even a single observatory is a time-honored method (Banks, 1969).

We use version 0130 of a database of hourly observatory data compiled and distributed by the British Geological Survey, which spans 1900 CE to the end of 2021 CE (Macmillan and Olsen, 2013). Observatories within 25° of the 2012 geomagnetic poles were eliminated to remove data contaminated by auroral fields (a more conservative cut-off of 35° is normally used, but we wanted to maximize the number of observatories contributing to our analysis). Any data gap of 48 h or less was bridged using linear interpolation (by far the most common gap was 24 h in length), and obvious data outliers were also replaced by interpolation. Baseline corrections were applied manually, guided by the thirteenth generation release of the International Geomagnetic Reference Field (Alken et al., 2021), to remove crustal biases for each observatory and to correct for occasional baseline shifts.

From the beginning of every year we selected all observatories that had 13 months of continuous data (i.e. having no data gaps) from that time, and carried out fits to $i_1^0(t)$ and $e_1^0(t)$ for that group of observatories. This produced a one month overlap between years that was used to remove the offsets between years caused by the changing distribution of observatories. Offsets were further reduced by removing the main signature of the core field using predictions for the internal part of the continuous COV-OBS.x2 internal field model (Huder et al., 2020), using a cubic spline interpolation over 10-year increments to avoid removing any signal at 11 years. This model, which has a 2 year knot spacing in its spline representation, was created specifically from quiet data to minimize external field variations, and thus provides a way to separate secular core field variations from the minimal remaining externally induced internal variations. There were a total of 180 observatories that had usable data (Fig. 3).

The result of this processing is two continuous time series from 1903 to 2021 CE of the internal and external magnetic dipole coefficients. The sum of these records is in many ways similar to the *Dst* magnetic index, an hourly estimate of P_1^0 ring current variations in the magnetic field derived from four low-latitude observatories (currently Kakioka, Honolulu, San Juan, and Hermanus), and if one plots the sum of our internal and external time series against *Dst* the result is indeed very similar (Fig. 4). However, there are several important differences between *Dst* and our data. First is that *Dst* data only go back in time to 1957 CE, while our data extend to 1903 CE. Second is that year-to-year baselines and the daily variation are removed in computing *Dst*, while our data can capture periods longer than one year and include the daily variations. Finally, *Dst* is a combination of the external and internal fields, while we have been able to make the separation by using data from a larger number of observatories that span a broader set of latitudes. Our results for the external field are comparable to those of Pick et al. (2019) who used geomagnetic observatory data from 34 locations to construct an hourly index of magnetospheric current variations (HMC) following removal of field models representing the core, crustal, and ionospheric solar-quiet field contributions.

The name *Dst* is short for "disturbed storm time", which provides insight into the main source of energy contributing to the observatory records (e.g. Daglis et al., 2007). Magnetic storms are caused by large increases in solar wind particles, which puts pressure on the dayside magnetic field and injects particles into the radiation belts that form the ring current at 2–9 Earth radii. These large expulsions of charged particles from the Sun's corona are associated with magnetic reconnection above sunspots. Magnetic storms are transitory events, lasting only a few days, but they are modulated by the solar rotation (27 days) moving sunspots into and away from the Earth–Sun axis. The number of magnetic storms is also modulated by the 11-year sunspot cycle, which provides power in the spectrum at these longer periods the way an amplitude modulated or pulse width modulated signal is used in radio and power systems. Fig. 4 illustrates the relationship between all these data sets.

Fig. 5 shows the combined field spectrum, along with the residual internal observatory spectrum, and spectra from COV-OBS.x2 and

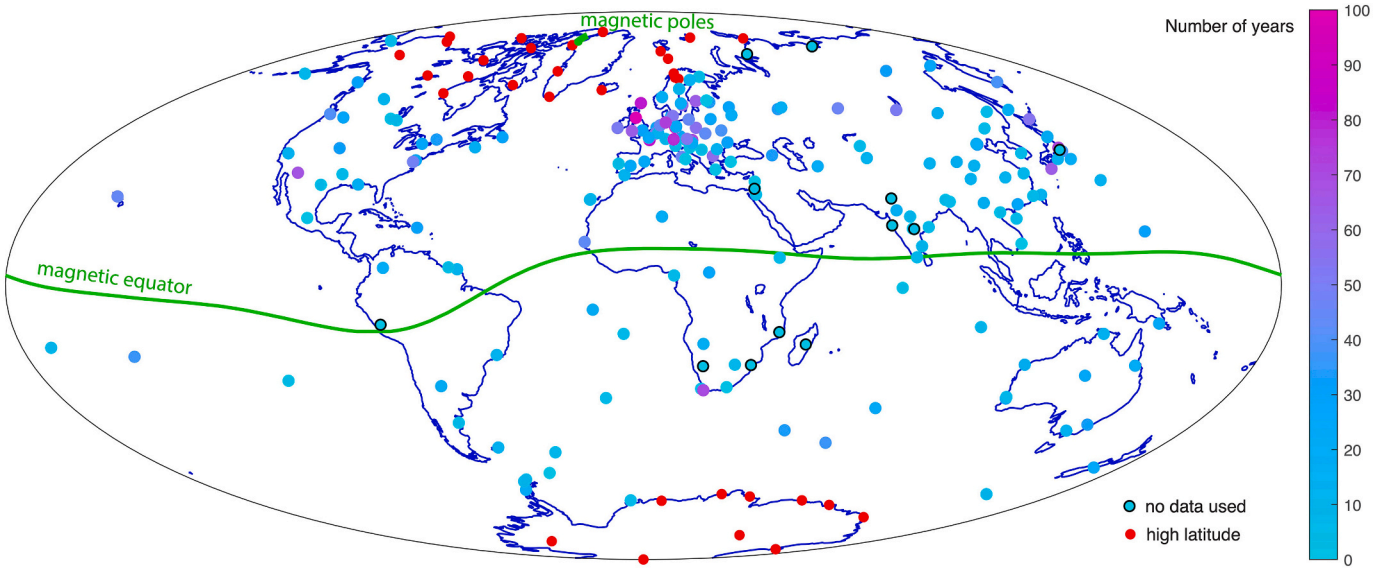

Fig. 3. Map of observatory distribution colored by number of years of data used. Twelve observatories had no usable data, and after elimination of observatories at high magnetic latitudes there were 180 usable sites.

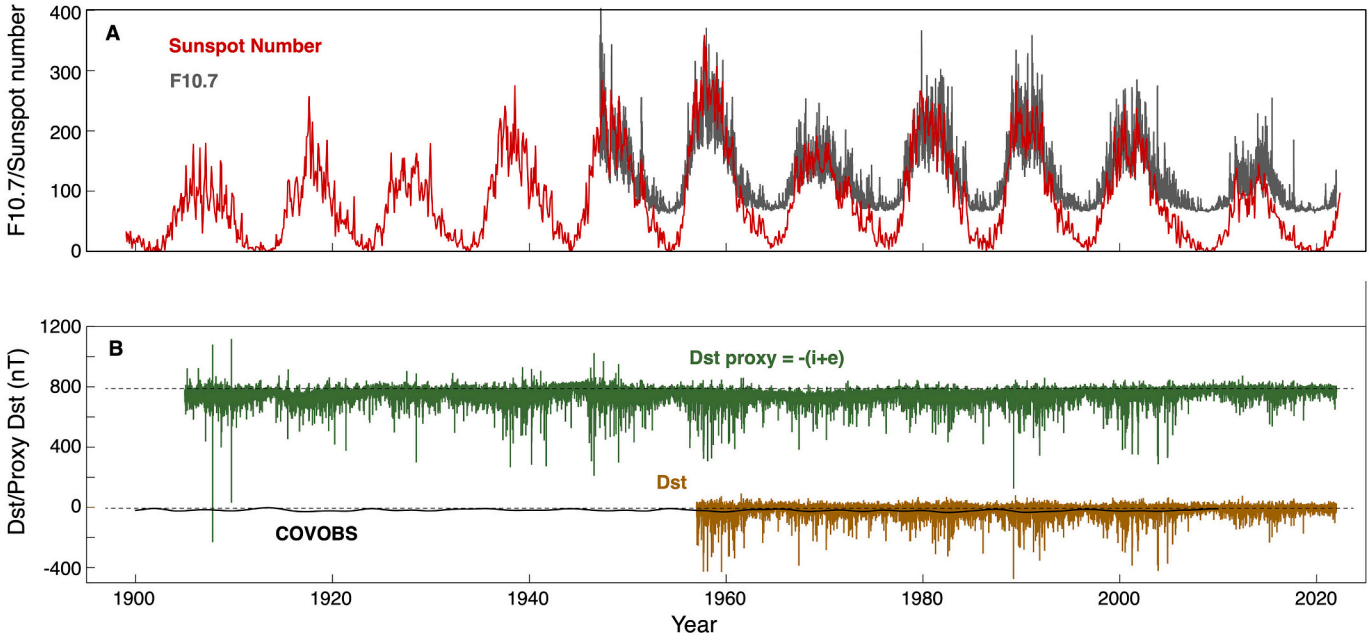

Fig. 4. (A) Time series of monthly sunspot number (World Data Center SILSO, Royal Observatory of Belgium, Brussels) and F10.7 solar radio flux (lasp.colorado.edu/lisird/data/noaa_radio_flux) reflecting solar cycle variations since 1900 and 1947 respectively. (B) Dst index since 1957 compared with our Dst proxy constructed from the sum of external and internal dipole coefficients (offset by 800 nT). The COV-OBS external model is shown for comparison.

CHAOS7 for comparison. The broad peaks at 27 days and harmonics are associated with solar rotation, as expected, and there are peaks visible at the 11-year sunspot cycle and second and third harmonics in the combined field spectrum with corresponding peaks in the internal field. There are also sharp peaks in the internal field spectrum at periods of 1.7 and 7.4 years. The peak at 1.7 years is clearly not present in the external field. The peak at 7.4 years is not strongly developed in the external field, but may be contributing to the shoulder of the broader 11 year peak. Oscillations at periods between 2 and 8.5 years in the magnetic field and length of day have been attributed to torsional Alfven waves and quasi-geostrophic magneto-Coriolis waves in the core (e.g., Rosat and Gillet, 2023), but while our observations may have some bearing on that subject, since these peaks do not contribute to the combined spectrum we will not consider them further.

The lines in the spectra at one year, six months, and daily harmonics do not reflect the P_1^0 source geometry dominant in the magnetosphere, but they serve to show that the magnetic field has significant power at these frequencies. It is also worth noting that, strictly speaking, as a delta function in frequency a line would not be properly represented in a spectral density plot. The daily variations result from electric currents driven by thermal tides in the ionosphere caused by heating on the dayside of Earth. Heating is greatest at the sub-solar point, which migrates between the hemispheres as seasons change, thus causing the variations at yearly and six monthly periods.

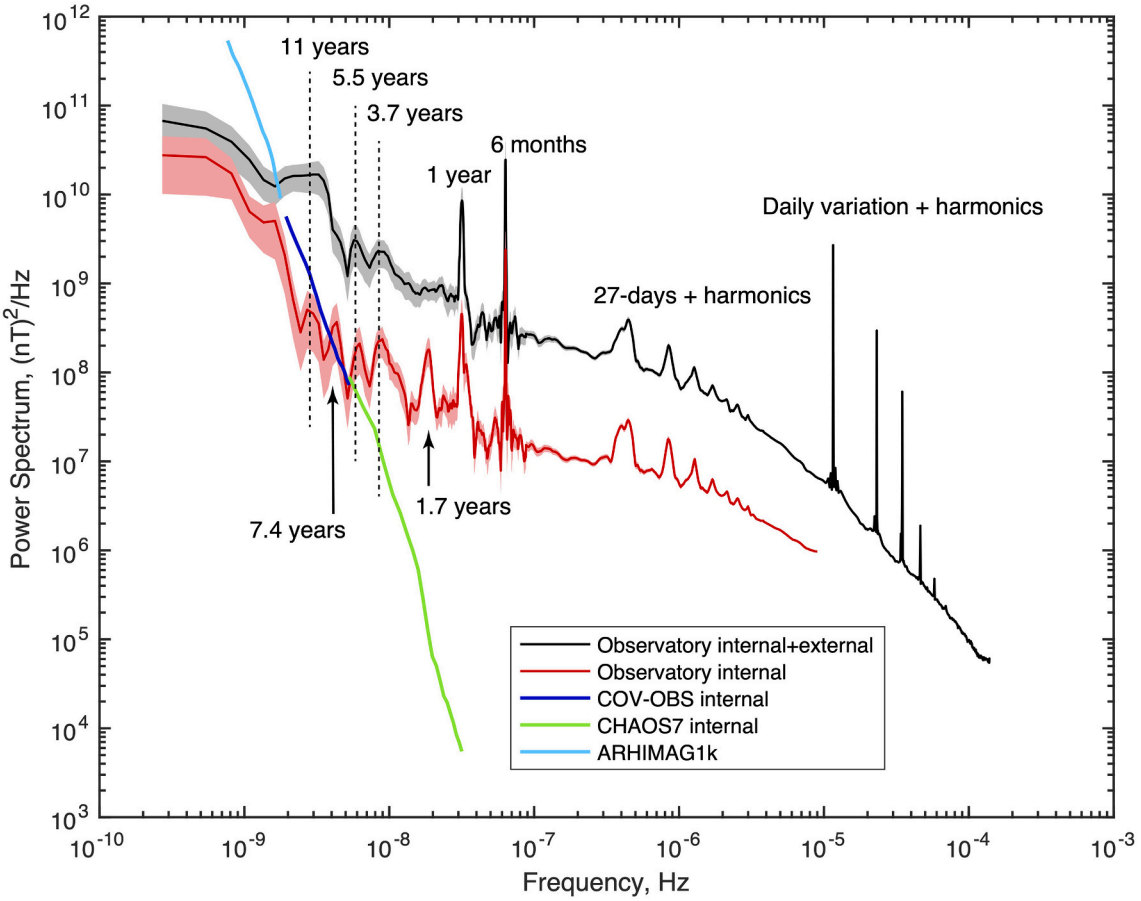

Fig. 5. Adaptive multi-taper spectrum of the combined internal plus external field coefficient time series (black, grey area gives 1 standard error) and the internal field (red, with light red 1 standard error) truncated at a period of one day. The amount of spectral smoothing is adjusted at periods of one day and 6 months to preserve resolution at long periods while reducing scatter at short periods. The internal spectra from COV-OBS.x2, CHAOS7, and ARHIMAG1k (Fig. 2) are plotted for comparison. (For interpretation of the references to colour in this figure legend, the reader is referred to the web version of this article.)

The observatory internal field spectrum is truncated at periods of one day and shorter because the P_1^0 geometry no longer dominates at these frequencies and our internal/external separation would not be valid. Between periods of one day and 11 years the internal field mimics many aspects of the combined field, which is dominated by the external field, reflecting the induced nature of the internal field at these frequencies. At periods longer than 11 years the internal field rises steeply towards the external field, indicating that it is no longer only an induced field, which is supported by its consistency with the COV-OBS.x2 estimate of the internal secular variation field estimated by using only quiet and night-time data. The CHAOS7 estimate of the internal field diverges from the induced internal field derived from observatory data at periods shorter than 4 years, highlighting the challenge inherent in recovering the internal core magnetic field contribution at these frequencies.

5. SYM-H

To analyze the external magnetospheric dipole variations at periods shorter than a day we turn to the higher resolution index, *SYM-H*, sampled at one minute intervals since 1981. It is similar to the *Dst* index (Wanliss and Showalter, 2006) but derived from six observatories whose makeup varies with data availability. In Fig. 6 we show a spectrum of 7.6 years of *SYM-H* data, which exhibits a bland $(1/f^2)$ slope with vestiges of the daily variation and first harmonic, bracketed by flattening at periods longer than 10 days and shorter than a few hundred seconds. The *Sq* daily variation, in the form of a 5 day average for each month, is intentionally removed from the *SYM-H* index, hence its signature is greatly reduced in Fig. 6. The calculation of *SYM-H*, as for *Dst*, makes no attempt to separate internal and external field contributions, and we see in Fig. 1 that the *SYM-H* spectrum can be joined seamlessly to the total field estimate from the observatory data.

6. 100 Seconds to 100 Hertz

To extend the spectrum to higher frequencies than 1 Hz, it is no longer practical to use global data. At these frequencies the external magnetic field is generally considered to be horizontal, and will vary both in time and location. However, by taking examples of data collected at mid-latitudes and averaging over several days we can obtain spectra that are representative and can be merged with the longer period parts of the spectrum. We can illustrate the temporal variability by including an example of data collected during a magnetic storm.

Data for frequencies around 1 Hz were collected using BF-4 induction coil sensors manufactured by EMI Inc. These sensors have been a standard for geophysical exploration, with a bandwidth between 1,000 s period and 1 kHz. Data were recorded at 500 Hz sample rate for several weeks 30 km east of Borrego Springs, California. A two hour recording of the magnetic north component was used to compute the spectrum shown in black in Fig. 7.

The first and third harmonics of the USA 60 Hz powerline frequency are evident, but also the first and fourth harmonics of 50 Hz at much lower amplitude, perhaps from local generators operating at the power frequency used in many other countries. Between 7 Hz and 50 Hz the Schumann resonances are clearly visible. These are resonant frequencies of the Earth-ionosphere waveguide, excited by global lightning strikes. The fundamental frequency, 7.7 Hz, is determined by the speed of light

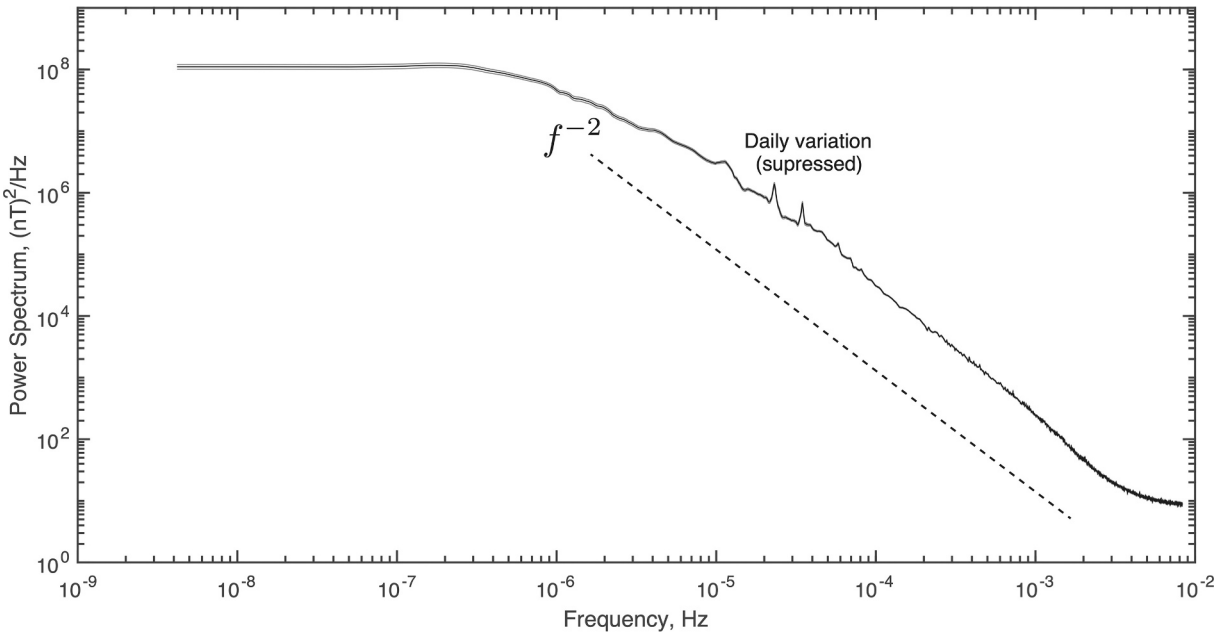

Fig. 6. Adaptive multi-taper spectrum of 7.6 years of SYM-H data.

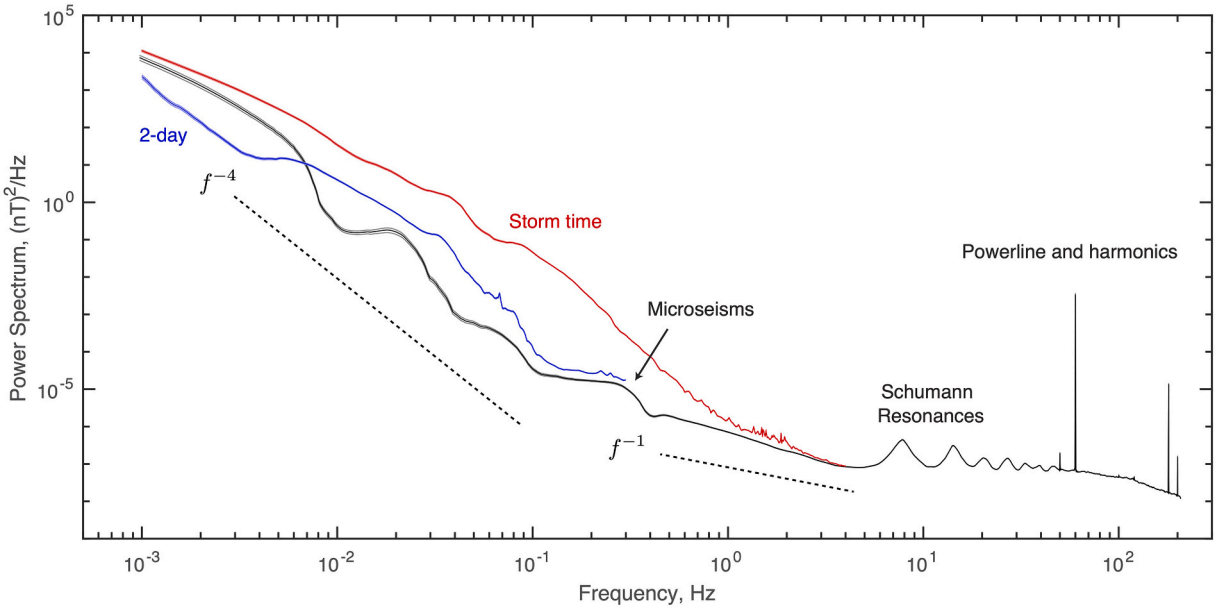

Fig. 7. Adaptive multi-taper spectrum of 2 h of induction coil data sampled at 500 Hz collected near Borrego Springs, California (black line) and for 2 days of data re-sampled at 5 Hz (blue line). Also shown is the spectrum of 12 h data collected at 50 Hz in South Australia during a 200 nT magnetic storm on May 4, 1998 (red line). (For interpretation of the references to colour in this figure legend, the reader is referred to the web version of this article.)

divided by Earth circumference, modified by the electrical conductivity of the ionosphere, which also broadens the peaks. The exact frequencies and amplitudes of the Schumann resonance will vary with time and location, as the height and conductivity of the ionosphere and the amount and distribution of lightning varies, but the seven harmonics visible here are representative of the phenomenon.

At frequencies lower than the Schumann resonance the field initially climbs as $1/f$, but steepens at around 0.1 Hz to $1/f^4$. The features in this part of the spectrum are variable in time, as micro-pulsations of the magnetic field come and go. Magnetic storms, associated with coronal mass ejections from the sun, can significantly increase power in this part of the magnetic spectrum. To illustrate this, we use data collected in South Australia as part of a global lightning study, described by Fullekrug and Constable (2000), and which fortuitously recorded a 200 nT magnetic storm on May 4, 1998. The spectrum of 12 h of these data, sampled at 50 Hz, is elevated over the quiet-time spectrum between 0.003 Hz to 3 Hz, and by as much as 3 orders of magnitude at 0.1 Hz (red line Fig. 7). To average out variability in the spectrum below 1 Hz and to improve statistical reliability, we took 2 days of Borrego data, high-cut filtered it with a corner frequency of 1 Hz, and resampled the time series at 5 Hz to reduce it to a size suitable for spectral analysis. The resulting spectrum (blue line) is the rather bland $1/f^4$ spectrum. The slight flattening at 0.01 Hz is consistent with that seen in the *SYM-H* spectrum.

The small, broad peak at around 0.3 Hz is probably associated with the double-frequency peak of microseismic energy, caused by wave-

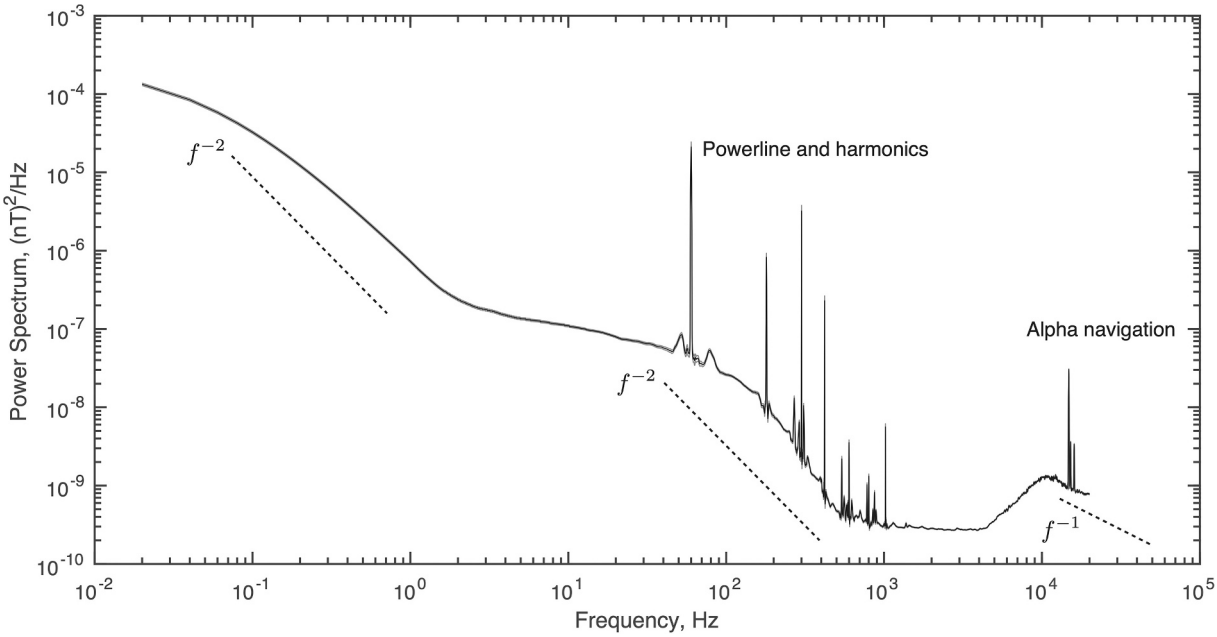

Fig. 8. Adaptive multi-taper spectrum of 50 s of induction coil data sampled at 40 kHz collected at Clark Dry Lake, California.

wave interaction in the oceans. This is not a feature of the magnetic field, but a result of seismic energy vibrating the induction coil sensors in Earth's main field. Since the main field is about 40,000 nT, it only takes a rotation of 10^{-7} radians, or ten millionth of a degree, to create a signal this large (∼0.003 nT).

7. Kilohertz frequencies

For the highest frequencies considered here, we use 50 s of magnetic field data sampled at 40 kHz collected in the region of Clark Dry Lake, Borrego Springs, California. These data were collected using a Quasar Federal Systems magnetic field sensor, an induction coil combined with a low-impedance amplifier (Tom Nielsen, personal communication, 2008). Dominating the spectrum (Fig. 8) are lines at the 60 Hz power line frequency and (mostly odd) harmonics up to the 17th. The peaks are broader and lower than for the 2-h record, probably because of the shorter sampling time. Other man-made signals are evident in the peaks at 14.78, 15.2, and 16.0 kHz associated with transmissions in the 12–16 kHz frequency range from the alpha navigation system (http://www.vlf.it/alphatrond/alpha.htm).

The broad peak at 10 kHz is characteristic of energy from global lightning return strokes, made more apparent by a maximum of the Earth-ionosphere waveguide attenuation at around 2 kHz, which has reduced the signal in the 1–4 kHz band. The flattening of the spectrum within this band may be a result of the noise floor of the measurement system. At high frequencies between 10 kHz and 100 kHz the field continues to fall off as $1/f$.

8. Summary

Collectively the spectra shown in Figs. 2–8 have been merged into the single product shown in Fig. 1, with areas of overlap trimmed at the longest and shortest periods. Dynamic changes in the spectrum highlight the range of influences on the magnetic field we measure. At the very longest periods, >30 My, we see the effects of changes in reversal rate and average reversal/excursion rates (100 ky-10 My). Between 100 ky and 100 yr we see the signature of paleosecular variation including the decay and recovery of the axial dipole before and after excursion and reversal. Spectral fall-off starts proportional to $1/f^2$ at 100 ky, and the core spectrum steepens to $1/f^6$ at the highest frequencies detectable for the core field. Significant external field variations driven by magnetic storms are visible for 11 years and shorter periods, and these overwhelm the signal from Earth's core, reducing the rate of fall-off, revealing periodic variations at 11 years and harmonics, and seasonal and daily variations attributable to ionospheric changes. A slight steepening is evident at <1 day periods, before a flattening and the transition to micropulsations signals. Another flattening is associated with microseisms, followed by further decay, the characteristic atmospheric signature from the Schumann resonances, and multiple contributions from anthropogenic noise.

CRediT authorship contribution statement

Catherine Constable: Conceptualization, Formal-analysis, Methodology, Writing-original-draft, Writing-review-editing. **Steven Constable:** Conceptualization, Data-curation, Formal-analysis, Methodology, Writing-original-draft, Writing-review-editing.

Declaration of Competing Interest

The authors declare that they have no known competing financial interests or personal relationships that could have appeared to influence the work reported in this paper.

Data availability

https://marineemlab.ucsd.edu/steve/projects/GrandSpectrum/index.html and https://earthref.org/ERDA/2719/

Acknowledgments

We thank Tom Nielsen for generously sharing the Quasar Federal Systems data collected at Borrego Springs, and Robert (Bob) Parker for providing his multi-taper spectral estimation code. This work was partly funded under NSF-NERC CSEDI grant EAR1953778. The authors also gratefully acknowledge hospitality and numerous collegial conversations during visits to GeoForschungsZentrum, Potsdam, Germany, and to the Isaac Newton Institute for Mathematical Sciences program on *Frontiers in Dynamo Theory: from the Earth to the Stars* in Cambridge, UK.

Financial support for these visits was provided by the Humboldt Foundation, and by EPSRC Grant No. EP/R014604/1. Two anonymous reviewers suggested a number of important clarifications to the original manuscript.

Images and data for the spectrum can be downloaded from.
https://marineemlab.ucsd.edu/steve/projects/GrandSpectrum/
and
https://earthref.org/ERDA/2719/

References

Alken, P., Erwan, T., Beggan, C., Amit, H., Aubert, J., Baerenzung, J., Bondar, T., Brown, W., Califf, S., Chambout, A., Chulliat, A., Cox, G., Finlay, C., Fournier, A., Gillet, N., Grayver, A., Hammer, M., Holschneider, M., Huder, L., Zhou, B., 2021. International geomagnetic reference field: the thirteenth generation. Earth, Planets and Space 73, 48. https://doi.org/10.1186/s40623-020-01281-4.

Backus, G., Parker, R.L., Constable, C., 1996. Foundations of Geomagnetism. Cambridge University Press, Cambridge England, New York.

Backus, G.E., 1983. Application of mantle filter theory to the magnetic jerk of 1969. Geophys. J. Roy. Astr. Soc. 74, 713–746. https://doi.org/10.1111/j.1365-246X.1983.tb01901.x.

Balasis, G., Egbert, G.D., 2006. Empirical orthogonal function analysis of magnetic observatory data: Further evidence for non-axisymmetric magnetospheric sources for satellite induction studies. Geophys. Res. Lett. 33 https://doi.org/10.1029/2006GL025721.

Banks, R., 1969. Geomagnetic variations and electrical conductivity of upper mantle. Geophys. J. Roy. Astronom. Soc. 17, 457–487. https://doi.org/10.1111/j.1365-246X.1969.tb00252.x.

Banks, R., Bullard, E., 1966. The annual and 27 day magnetic variations. Earth Planet. Sci. Lett. 1, 118–120.

Barton, C., 1982. Spectral analysis of palaeomagnetic time series and the geomagnetic spectrum. Phil. Trans. R. Soc. Lond. A306, 203–209. URL: https://www.jstor.org/stable/37197.

Constable, C., 2016. Earth's electromagnetic environment. Surv. Geophys. 37, 27–45. https://doi.org/10.1007/s10712-015-9351-1.

Constable, C., 2019. Temporal field variations: from reversals to very-low-frequency waves. In: Mandea, M., Korte, M., Yao, A., Petrovsky, E. (Eds.), Geomagnetism, Aeronomy and Space Weather. Cambridge, pp. 181–185. https://doi.org/10.1017/9781108290135.

Constable, C., Johnson, C., 2005. A paleomagnetic power spectrum. Phys. Earth Planet. Inter. 153, 61–73. https://doi.org/10.1016/j.pepi.2005.03.015.

Constable, C., Korte, M., Panovska, S., 2016. Persistent high paleosecular variation activity in southern hemisphere for at least 10000 years. Earth Planet. Sci. Lett. 453, 78–86. https://doi.org/10.1016/j.epsl.2016.08.015.

Constable, C.G., Constable, S.C., 2004. Satellite magnetic field measurements: applications in studying the deep earth. In: The state of the planet: frontiers and challenges in geophysics. American Geophysical Union; Washington, DCS.l., pp. 147–159. doi:10.1029/150GM13.

Constable, C.G., Tauxe, L., Parker, R.L., 1998. Analysis of 11 Myr of geomagnetic intensity variation. J. Geophys. Res.-Solid Earth 103, 17735–17748. https://doi.org/10.1029/98JB01519.

Constable, S.C., Parker, R.L., Constable, C.G., 1987. Occam's inversion: a practical algorithm for generating smooth models from electromagnetic sounding data. Geophysics 52, 289–300. URL: doi: 10.1190/1.1442303, doi:10.1190/1.1442303.

Courtillot, V., Le Mouël, J.L., 1988. Time variations of the earth's magnetic field: from daily to secular. Annu. Rev. Earth Planet. Sci. 16, 389–476. https://doi.org/10.1146/annurev.ea.16.050188.002133.

Daglis, I.A., Tsurutani, B.T., Gonzalez, W.D., Kozyra, J.U., Orsini, S., Cladis, J., Kamide, Y., Henderson, M.G., Vassiliadis, D., 2007. Key features of intense geospace storms—a comparative study of a solar maximum and a solar minimum storm. Planet. Space Sci. 55, 32–52. https://doi.org/10.1016/j.pss.2006.04.007.

Eckhardt, D., Larner, K., Madden, T., 1963. Long-period magnetic fluctuations and mantle electrical conductivity estimates. J. Geophys. Res. 68, 6279–6286.

Everett, M., Constable, S., Constable, C., 2003. Effects of near-surface conductance on global satellite induction responses. Geophys. J. Int. 153, 277–286. https://doi.org/10.1046/j.1365-246X.2003.01906.x.

Finlay, C.C., Kloss, C., Olsen, N., Hammer, M., Tøffner-Clausen, L., Grayver, A., Kuvshinov, A., 2020. The CHAOS-7 geomagnetic field model and observed changes in the south atlantic anomaly. Earth, Planets and Space 72, 156. https://doi.org/10.1186/s40623-020-01252-9.

Fullekrug, M., Constable, S., 2000. Global triangulation of intense lightning discharges. Geophys. Res. Lett. 27, 333–336. https://doi.org/10.1029/1999GL003684.

Gillet, N., Jault, D., Finlay, C.C., Olsen, N., 2013. Stochastic modeling of the earth's magnetic field: Inversion for covariances over the observatory era. Geochem. Geophys. Geosyst. 14 https://doi.org/10.1002/ggge.20041.

Huder, L., Gillet, N., Finlay, C.C., Hammer, M.D., Tchoungui, H., 2020. Cov-obs.x2: 180 years of geomagnetic field evolution from ground-based and satellite observations. Earth, Planets and Space 72, 160.

Jackson, A., Jonkers, A.R.T., Walker, M.R., 2000. Four centuries of geomagnetic secular variation from historical records. Phil. Trans. R. Soc. Lond. A 358, 957–990. https://doi.org/10.1098/rsta.2000.0569.

Lanzerotti, L., Mclennan, C., Fraser-Smith, A., 1990. Background magnetic spectra: $\sim 10^{-5}$ to $\sim 10^{5}$ hz. Geophys. Res. Lett. 17, 1593–1596. https://doi.org/10.1029/GL017i010p01593.

Macmillan, S., Olsen, N., 2013. Observatory data and the swarm mission. Earth, Planets and Space 65, 1355–1362. https://doi.org/10.5047/eps.2013.07.011.

Mandea, M., Holme, R., Pais, A., Pinheiro, K., Jackson, A., Verbanac, G., 2010. Geomagnetic jerks: Rapid core field variations and core dynamics. Space Sci. Rev. 155, 147–175. https://doi.org/10.1007/s11214-010-9663-x.

Ogg, J., Smith, A., 2012. Chapter 5 - geomagnetic polarity time scale. In: Gradstein, F.M., Ogg, J.G., Schmitz, M.D., Ogg, G.M. (Eds.), The Geologic Time Scale. Elsevier, Oxford, pp. 85–113. https://doi.org/10.1016/B978-0-444-59425-9.00005-6.

Olsen, N., 2007. Natural sources for electromagnetic induction studies. In: Gubbins, D., Herrero-Bervera, E. (Eds.), Encyclopedia of Geomagnetism and Paleomagnetism. Springer, pp. 696–700.

Olsen, N., Kuvshinov, A., 2004. Modeling the ocean effect of geomagnetic storms. Earth Planets and Space 56, 525–530. https://doi.org/10.1186/BF03352512.

Panovska, S., Constable, C.G., Korte, M., 2018. Extending global continuous geomagnetic field reconstructions on timescales beyond human civilization. Geochem., Geophys., Geosyst., 1559–1580. URL: doi: 10.1029/2017GC007271, doi:10.1029/2017GC007271.

Panovska, S., Korte, M., Constable, C.G., 2019. One hundred thousand years of geomagnetic field evolution. Rev. Geophys., 1289–1337. URL: https://doi.org/10.1029/2019RG000656, doi:10.1029/2019RG000656.

Pick, L., Korte, M., Thomas, Y., Krivova, N., Wu, C.J., 2019. Evolution of large-scale magnetic fields from near-earth space during the last 11 solar cycles. J. Geophys. Res. Space Phys. 124, 2527–2540. https://doi.org/10.1029/2018JA026185.

Pinheiro, K., Jackson, A., 2008. Can a 1-d mantle electrical conductivity model generate magnetic jerk differential time delays? Geophys. J. Int. 173, 781–792. https://doi.org/10.1111/j.1365-246X.2008.03762.x.

Riedel, K.S., Sidorenko, A., 1995. Minimum bias multiple taper spectrum estimation. IEEE Trans. Signal Proces. 43, 188–195. https://doi.org/10.1109/78.365298. URL: https://ieeexplore.ieee.org/stamp/stamp.jsp?tp=&arnumber=365298.

Riedel, K.S., Sidorenko, A., 1996. Adaptive smoothing of the log spectrum with multiple tapering. IEEE Trans. Signal Proc. 44, 1794–1800. https://doi.org/10.1109/78.510625. URL: https://ieeexplore.ieee.org/stamp/stamp.jsp?arnumber=510625.

Rosat, S., Gillet, N., 2023. Intradecadal variations in length of day: coherence with models of the earth's core dynamics. Phys. Earth Planet. Inter. 341 https://doi.org/10.1016/j.pepi.2023.107053.

Sadhasivan, M., Constable, C., 2022. A new power spectrum and stochastic representation for the geomagnetic axial dipole. Geophys. J. Int. 231, 15–26. https://doi.org/10.1093/gji/ggac172.

Senftleben, R., 2020. Earth's magnetic field over the last 1000 years. Ph.D. thesis. University of Potsdam. URL: https://doi.org/10.25932/publishup-47315.

Wanliss, J.A., Showalter, K.M., 2006. High-resolution global storm index: Dst versus symh. J. Geophys. Res.: Space Phys. 111 https://doi.org/10.1029/2005JA011034. URL: https://agupubs.onlinelibrary.wiley.com/doi/abs/10.1029/2005JA011034.

Ziegler, L.B., Constable, C.G., Johnson, C.L., Tauxe, L., 2011. PADM2M: a penalized maximum likelihood model of the 0–2 Ma palaeomagnetic axial dipole moment. Geophys. J. Int. 184, 1069–1089. https://doi.org/10.1111/j.1365-246X.2010.04905.x.